Near field enhancement and absorption properties of the double cylindrical microcavities based on triple-band metamaterial absorber

Heng Hang(衡 航)[a)b)†] and Yang Li(杨 理)[a)]

[a)] Department of Physics, Nanjing Normal University, Nanjing 210097, China
[b)] Center for Analysis and Testing, Nanjing Normal University, Nanjing 210097, China

(Received 12 November 2013; revised manuscript received 16 December 2013; published online 10 April 2014)

We numerically study the near field enhancement and absorption properties inside the double cylindrical microcavities based on triple-band metamaterial absorber. The compact single unit cell consists of concentric gold rings each with a gold disk in the center, and a metallic ground plane separated by a dielectric layer. At the normal incidence of electromagnetic radiation, the obtained reflection spectra show that the resonance frequencies of the double microcavities are 16.65 THz, 20.65 THz, and 25.65THz, respectively. We also calculate the values of contrast C ($C = 1 - R_{\min}$), which can reach 95%, 97%, and 95% at the corresponding frequencies by optimizing the geometry parameters of structure. Moreover, we demonstrate that the multilayer structure with subwavelength electromagnetic confinement allows $10^4 \sim 10^5$-fold enhancement of the electromagnetic energy density inside the double cavities, which contains the most energy of the incoming electromagnetic radiation. Moreover, the proposed structure will be insensitive to the polarization of the incident wave due to the symmetry of the double cylindrical microcavities. The proposed optical metamaterial is a promising candidate as an absorbing element in scientific and technical applications because of its extreme confinement, multiband absorptions, and polarization insensitivity.

Keywords: metamaterial, metal–semiconductor–metal, microcavity, absorption

PACS: 81.05.Xj, 42.55.Sa, 73.40.Sx, 78.67.Pt **DOI:** 10.1088/1674-1056/23/6/068101

1. Introduction

Optical metamaterials are composite structures composed of nanoscale resonators organized to give a highly customized electric and magnetic response in a specific wavelength range of interest.[1] Benefitting from free geometries and compositions, metamaterials have presented extraordinary optical properties such as surface-enhanced spectroscopy,[2–4] enhanced transmission,[5–7] sensitive bio-sensing,[8,9] negative refractive index,[10–12] and high resolution imaging.[13,14] In the visible and near infrared range,[15,16] surface-plasmon polaritons (SPPs) and localized surface polaritons (LSPs) have become the theoretical basis for the research of optical metamaterials. As the wavelength increases, the penetration depth into the dielectric layer increases, ohmic loss of the metal layer reduces reversely, and, in particular, in far infrared, ohmic loss is very low, and it has a perfect reflection characteristic. Because of these features, the diffraction limit can be broken and light can be confined within a subwavelength volume. In recent years, one of the hot issues in optical metamaterial research is to confine light within the subwavelength. Today, antennas are widely used in microwave,[17] and nano-antenna devices have been explored in up to the visible range.[18,19] Fevillet–Palma[20] have studied the near-field enhancement properties of THz antenna microcavities, also in THz. The dimensions of cavities can be reduced to high subwavelength, owing to low ohmic loss in the metal layer and perfect absorption in the dielectric layer.[21,22] Moreover, the parameters of the structure must be optimized to effectively match the impedance of the structure with that of a vacuum. Much work about optical metamaterials has been reported in the mid-infrared range, but, so far, little literature focuses on the field-enhancement properties of metal–dielectric–metal (MDM) sandwich resonant cavities. These MDM sandwich structures have the advantages in strong absorption and extreme confinement. In Ref. [20], "microcavities" have been originally proposed, and the field enhancement of the cuboid microcavities has been demonstrated in THz. Compared with previously reported literature, this kind of resonant structure can localize the electromagnetic energy into the symmetrical cuboid with a size much smaller than the wavelength, and we can accurately calculate the electromagnetic energy density in the cavities. However, this structure has only single microcavities and a smaller value of C (85%). Furthermore, this cuboid microcavity is sensitive to the polarization of the incident wave. In this paper, we perform numerical simulations by using a commercial software, i.e., high frequency structure simulator (HFSS) to investigate the near-field enhancement and absorption properties of the double cylindrical microcavities based on triple-band metamaterial absorber. Besides the extreme confinement of the electromagnetic field within the cylinder cavities and strong absorption characteristics, since the concentric gold rings each with a gold disk in the center

†Corresponding author. E-mail: 40383@njnu.edu.cn

© 2014 Chinese Physical Society and IOP Publishing Ltd

are of circular symmetry, the insensitivity of the structure to polarization of the incident light is also investigated. For the proposed structure, the C and the energy density ratio Q can reach maximum values of 97% and $10^4 \sim 10^5$, respectively.

2. Simulation, structures, results, and discussion

The designed double MDM sandwich resonant cavities are simulated by HFSS, a finite element method-based program. The MDM cylindrical cavities are periodically arranged in a square lattice in the X–Y plane. Figure 1(a) shows the schematic plot of a unit cell of the double cylindrical cavities array. A dielectric layer is sandwiched between two metallic layers, the top layer is a concentric gold ring with a gold disk in the center and the bottom layer is the gold ground layer. The areas denoted with "V" in Fig. 1(a) represent the double cylindrical microcavities formed between the top patterned layer and a continuous gold layer. If the dielectric layer thickness L is smaller than the wavelength, such a structure supports a TM_{100} mode.[19] Cross section of the cavities in the X–Y plane is shown in Fig. 1(b). Figure 1(c) shows the cross section of the cavities in the Y–Z plane, and the structural parameters are shown in Figs. 1(b) and 1(c). The thickness of the GaAs layer is chosen as L, and r_1, r_2, r_3, and r_4 are defined as the radii of the middle gold disk, outer ring, inner ring, and the double cylindrical microcavities, respectively. The double cylindrical microcavities are located in the dielectric layer which can be called "hot volume", similar to "hot spot", highly confining the electromagnetic energy inside the microcavities. In this work, $H = 0.45$ μm, which is the same as the thickness of the middle gold disk. The gold ground layer has two significant functions. One is to serve as an optical mirror. As the thickness is greater than the penetration depth of the incident light, the transmittance is close to zero. The other is to couple the top patterned layer with the gold ground layer to create electric and magnetic dipoles which extremely concentrate electromagnetic energy into the microcavities. Period P is kept to be 6 μm. The orientations of the electric field ($\boldsymbol{E}$), the magnetic field ($\boldsymbol{H}$), and the wave vector ($\boldsymbol{K}$) are shown in Fig. 1(a). The incident angle is 0. The boundary conditions are set as the ones of perfect electric conductor and perfect magnetic conductor on two pair faces. The dielectric permittivity of gold is modeled using the Drude model:

$$\varepsilon = 1 - \frac{\omega_{\mathrm{p}}^2}{\omega^2 + \mathrm{i}\omega\gamma}, \tag{1}$$

with plasma frequency $\omega_{\mathrm{p}} = 1.37 \times 10^{16}$ rad/s and scattering frequency $\gamma = 4.08 \times 10^{13}$ rad/s. The refractive index of the dielectric layer is 3.55.

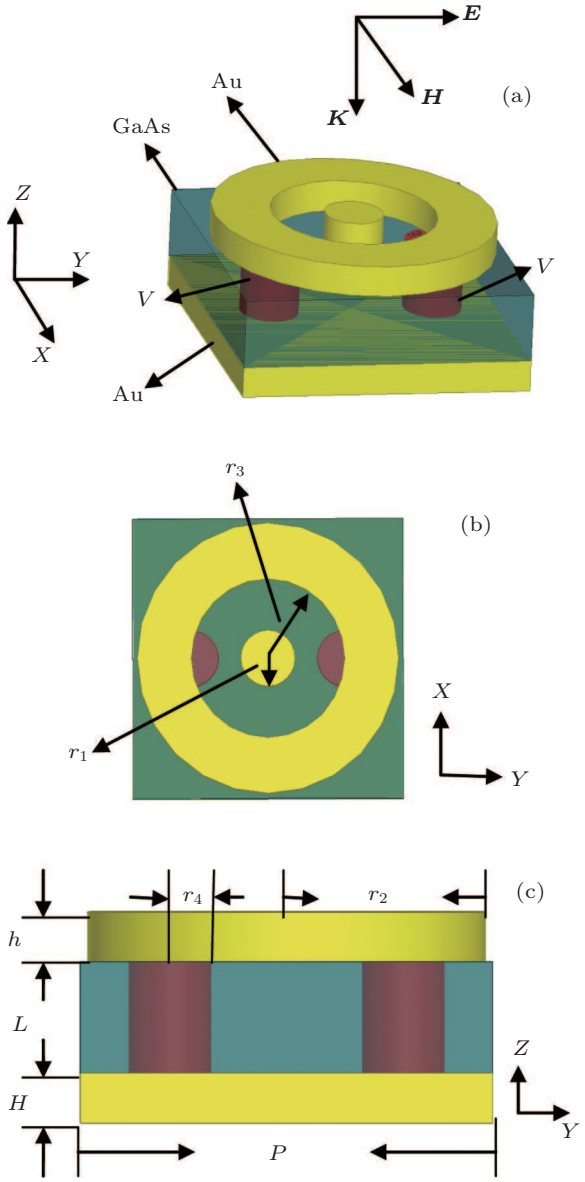


Fig. 1. (color online) Schematic diagram of a unit cell of the double cylindrical cavities array. (a) Schematic geometry of a unit cell of cylindrical microcavities at normally incident TM plane wave. The top is the concentric gold ring with a gold disk in the center, the middle dielectric layer is GaAs, the bottom is gold plane layer and the red areas are the double cylindrical microcavities. (b) Cross section view of the cylindrical microcavities in the X–Y plane. (c) Cross section view of the cylindrical microcavities in the Y–Z plane.

In order to study the resonant characteristics of cylindrical microcavities, we calculate the reflectivity spectra: $R(\omega) = |S_{11}(\omega)|^2$ of normally incident TM plane wave. As shown in Fig. 2, the resonant cavity mode appears as a reflection dip in the spectrum. Moreover, the grating period is kept at subwavelength, so that the only contribution to the reflected signal is the specular reflection (0th diffraction order).[20] We also calculate the transmission of the structure and obtain near zero transmission for all geometric parameters (transmission spectra are not given here). According to the following equation:

$$T + R + A = 1, \tag{2}$$

where T, R, and A are the transmission, reflection, and ab-

sorption, respectively. Due to $T = 0$, the minimum of reflection appears as the maximum of absorption. If we define $C = 1 - R_{\min}$, where $R_{\min}$ is the reflectivity minimum at the resonant frequency, a larger C indicates a stronger absorption.

Figure 2 shows the reflectivity (green) as well as those of the concentric rings and the middle disk alone. There are three reflection dips at frequencies 16.65 THz, 20.65 THz, and 25.65 THz with the values of C 95%, 97%, and 95%, respectively. The curves a and b represent the reflectivity values of the solely concentric rings and the middle disk, respectively. They match well with their composite's responses to blueshift for the peak of higher frequency and the other two peaks of lower frequencies remain unchanged. The response of the composite is not only the sum of that of each single component because of the coupling between the components. Furthermore, the resonant frequency can be designed to be the frequencies of interest by varying the structural parameters. Since the unit cell is of circular symmetry, it has the same response to transverse electric (TE) and transverse magnetic (TM) for normally incident EM wave.

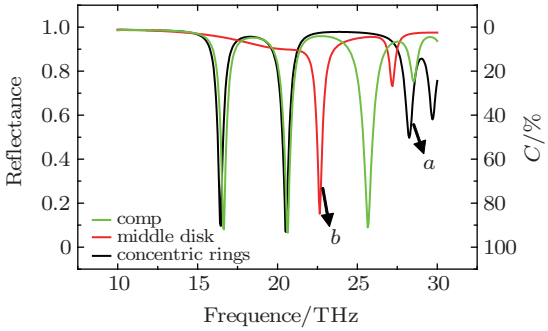


Fig. 2. (color online) Reflectivity spectra of the double cylindrical microcavities in the MDM structure at normally incident TM plane wave. The black, red, and green curves represent the reflectivity of the solely concentric gold rings, the middle disk, and their composite, respectively.

Figure 3(a) shows the reflectivity spectra of the double cylindrical microcavities in the MDM structure at normal incidence with variable radius r_1 and fixed $L = 1$ μm, $r_2 = 2.9$ μm, and $r_3 = 1.7$ μm. When the radius r_1 is changed from 0.5 μm to 0.75 μm in steps of 0.05 μm, the reflection peaks each show a red-shift with the increasing of r_1 at higher frequency, but at the two lower frequencies, the peaks stay nearly the same. The shifts of the reflectivity spectra result from the coupling between neighboring components. This near-field coupling phenomenon has been reported in Ref. [21]. As radius r_1 increases, the values of C keep over 90%. When r_1 is 0.6 μm, the resonant peaks are located at 18 μm, 14.5 μm, and 11.7 μm, however, the values of C reach 95%, 97%, and 95%, respectively. Like Fig. 3(a), figures 3(b) and 3(c) show the reflectivity spectra of the double cylindrical microcavities with variable r_2 and r_3. As shown in Figs. 3(b) and 3(c), the changes of r_2 and r_3 can also lead to the shift of the peak. This is because the changes of parameters in the top patterned layer result in a shift of the electric resonance frequency, thereby changing the effective dielectric permittivity $\varepsilon(\omega)$ of the system.

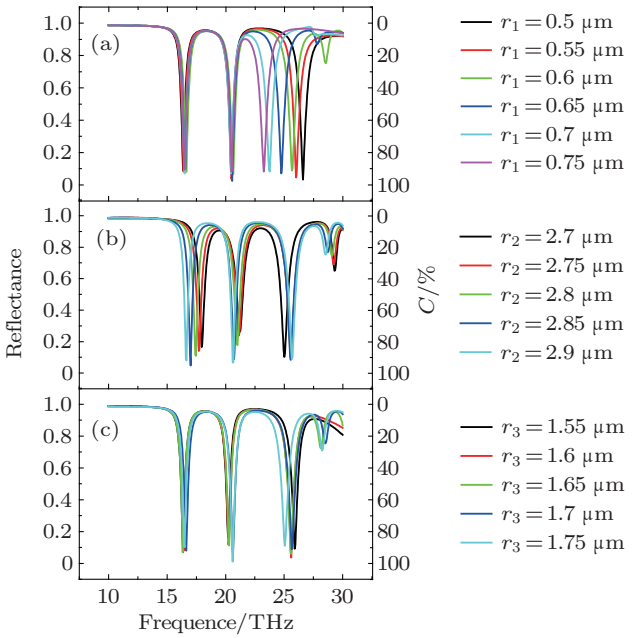


Fig. 3. (color online) Reflectivity spectra of the double cylindrical microcavities in the MDM structure at normally incident TM plane wave. (a) Reflectivity spectra at different values of r_1, $r_2 = 2.9$ μm, and $r_3 = 1.7$ μm. (b) Reflection spectra at different values of r_2, $r_1 = 0.6$ μm, and $r_3 = 1.7$ μm. (c) Reflectivity spectra at different values of r_3, $r_1 = 0.6$ μm, and $r_2 = 2.9$ μm.

So it is necessary to investigate our triple-band absorber by changing the dimensions of the concentric rings each with a disk in the center, thereby repositioning the reflectivity peaks while keeping their triple-band characteristics unchanged. Figure 4(a) shows that a 1.3-μm tunable range of resonant frequency can be achieved by engineering the sizes of the gold nanoparticles on the top layer, with the parameters of the concentric ring kept unchanged. For $r_1 = 0.6$ μm and $r_1 = 0.75$ μm, their corresponding values of C are equal and reach 97% at the resonant frequencies 26.65 THz and 23.25 THz, respectively. Increasing the radius r_1 of the middle disk causes a red shift of the reflectivity peaks, which is due to a decrease in space between particles, resulting in stronger coupling effect. When r_1 is kept within 0.6 μm, we increase r_2 from 2.8 μm to 2.9 μm and reduce r_3 from 1.7 μm to 1.65 μm as shown in Fig. 4(b), reflectivity peaks at the two lower frequencies simultaneously have red shifts. But at higher frequency, reflectivity peaks stay the same. We also investigate triple band control by changing the sizes of the concentric rings and the middle disk. The result in Fig. 4(c) shows that the three reflectivity peaks could simultaneously be adjusted, which indicates the great flexibility of our triple-band absorber in the mid-infrared range.

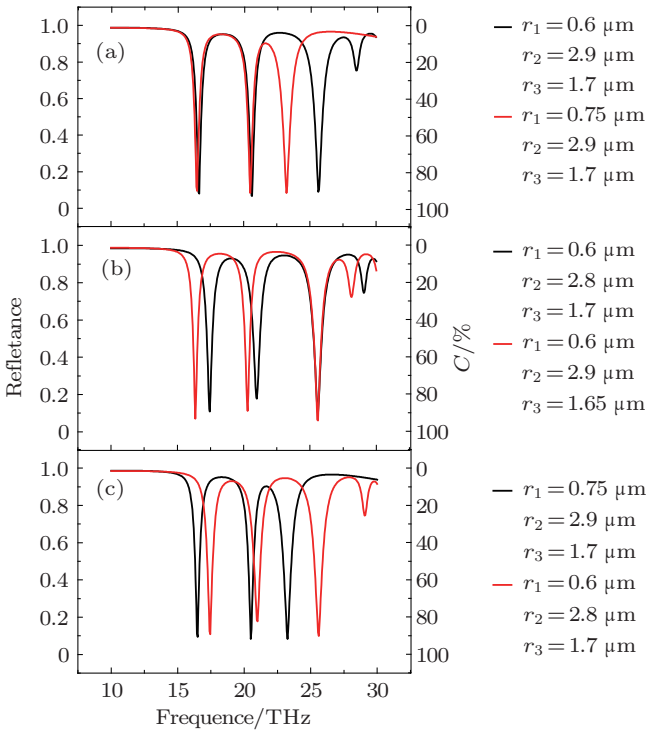


Fig. 4. (color online) Reflectivity spectra of the double cylindrical microcavities in the MDM structure with different dimensions of the top patterned gold nanoparticles. A 1.3-μm tunable range can be conveniently achieved by engineering the sizes of the gold nanoparticles on the top layer. (a) The higher frequency, (b) the two lower frequencies, and (c) the three reflectivity peaks can be easily tuned.

For the MDM structure studied in this case, the energy of incident wave is dissipated by both the metallic and the dielectric losses. Particularly in infrared wave bands, ohmic loss is low, and dielectric loss accounts for a large part of the energy, so C can reach high values. To prove this, we calculate the energy density of the electromagnetic field inside the double cavities. The double cylindrical microcavities are symmetrical for the unit cell, so we choose the left or right cavity in the Y-axis direction to compute the energy density. Because of energy conservation, the peak electrical energy is equal to the average total energy inside the cavity, and the solution is achieved by integrating $\boldsymbol{E}\cdot\boldsymbol{E}^*$ within the volume as follows:

$$E_{\mathrm{d}} = \int_V \frac{\boldsymbol{E}\cdot\boldsymbol{E}^*}{V}\mathrm{d}v, \tag{3}$$

where v is the volume of the cavity, E_{d} is the energy density inside the cavity, $\boldsymbol{E}$ represents the electric field vector inside the cavity. First, we calculate the energy density E_{d1} inside the GaAs cavity in the MDM structure. Then, we calculate the energy density E_{d2} inside the vacuum cavity without the MDM structure, whose shape and size are the same as those inside the GaAs cavity. We define $Q = E_{\mathrm{d1}}/E_{\mathrm{d2}}$ as the enhancement factor of energy density. The volume of the cavity will affect the EM energy absorption and confinement inside the cavity,[21] only when parameters of geometry are optimized and the impedance of the structure matches with the impedance of vacu μm, will the extreme confinement of EM field and strong absorption inside cavities appear. Figure 5 shows the energy density ratio Q as a function of r_4, where $r_1 = 0.6$ μm, $r_2 = 2.9$ μm, and $r_3 = 1.7$ μm. As shown in Fig. 5, when r_4 is increased from 0.01 μm to 0.6 μm, Q decreases linearly from 10324 to 6304. The results show that the absorption and confinement inside the cavity are sensitive to the radius of the cavity. At r_4=0.01 μm, Q reaches $\sim 10^4$. In the limit of the radius of the cavity $r_4 \to 0$, we can obtain higher Q. When $r_4 = 0$, the cavity becomes a "hot spot". For the surface-enhanced infrared spectroscopy (SEIRS) technique, the overall response is proportional to Q. So this structure is a good substrate for SEIRS because of high energy density ratio, multi-band absorption, and flexibility of adjusting resonant peaks. In order to explain the regularity of the value Q varying with r_4, we use the model (for the detailed derivations, refer to Ref. [20]):

$$\frac{\varepsilon|E_{Z0}|^2}{|E_{\mathrm{in}}|^2} = \frac{\lambda_{\mathrm{res}}\Sigma}{2\pi V}S_{\mathrm{ohm}}C\cos\theta \tag{4}$$

to describe the energy density ratio in the cavity, where $\varepsilon = 12.6$ is the dielectric constant of GaAs, $V = \pi r^2 L$ is the volume of the cylindrical resonator, E_{in} is the electric field amplitude of the incoming wave, E_{Z0} is the amplitude of the mode resonantly excited in the microcavity, and θ is the incident angle. For the data reported here we have $\cos\theta = 1$, $\Sigma = P^2$, S_{ohm} is the quality factor S of the ohmic loss. Because the values of Q_{ohm}, λ_{res}, and C are identical in the different structures as shown in Fig. 5, we can obtain $\varepsilon|E_{Z0}|^2/|E_{\mathrm{in}}|^2 \sim 1/V$, indicating that the energy density ratio inside the cavity is decided by $1/V$. Obviously, the conclusion of the analytical model is in good agreement with our calculation.

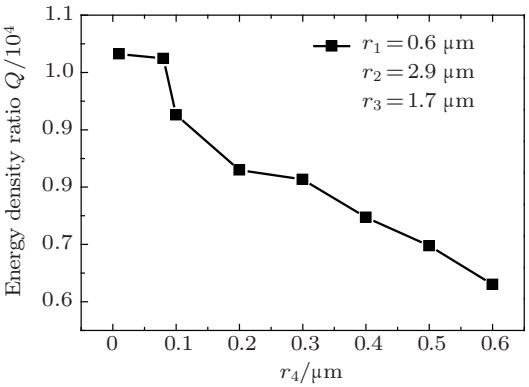


Fig. 5. Variation of ratio between the electromagnetic densities of the microcavity field and the field of the incoming plane wave with r_4, at $r_1 = 0.6$ μm, $r_2 = 2.9$ μm, and $r_3 = 1.7$ μm.

To explore the physical mechanism of the extreme confinement and perfect absorption inside the double cavities, the distributions of the EM field intensity and current at the resonant mode are simulated, and the results are shown in Fig. 6. Figure 6(a) shows the amplitude of electric field in the middle of the dielectric layer in the X–Y plane. The thin circles represent the double cylindrical microcavities, concentric rings, and the middle disk. Two standing wave patterns are clearly

shown in Fig. 6(a). The amplitude of the electric field can be approximated by the following expression:

$$|\boldsymbol{E}| \sim \cos\left(\pi X/\Delta x\right) \quad (0 \leq X < r). \tag{5}$$

At $r = 0$, $|\boldsymbol{E}|$ reaches its maximum, that is, energy is strongly localized around the center of the cylindrical microcavity, which is in good agreement with Fig. 5. Figure 6(b) shows the amplitude of electric field at the top surface of the dielectric layer in the X–Y plane. As indicated in Fig. 6(b), the distribution of electric field mainly concentrates at the two edges of the circumference of the inner ring, forming a two-crescent pattern in the Y-axis direction, which is caused by the rod effect.[22] In Fig. 6(c), the areas denoted with "M" represents the metal, the middle layer is dielectric and the EM field is highly localized between the two metal layers, in particular, most of the EM energy concentrates into the double symmetrical cylindrical microcavities, which has been proved by calculating the energy density Q. Figure 6(d) is the distribution of the magnetic field in the middle of the dielectric layer in the Y–Z plane. The areas denoted with "M" in this figure represent the two metal layers. The magnetic field distribution shown in Fig. 6(d) clearly indicates that the magnetic field is localized between two metal layers, meanwhile, stronger localization of the magnetic field appear underneath the middle gold disk, thus forming the magnetic dipole resonance. Therefore, both the parameters of the top gold layer and the thickness value of dielectric layer can be optimized to effectively match the impedance of the structure ($Z = \sqrt{\varepsilon(\omega)/\mu(\omega)}$) with that of a vacuum, and strongly coupling the incident radiation to the resonant structure.

As previously mentioned there are shifts of the triple-band reflectivity peaks with respect to those of the concentric rings and the middle disk alone, the physical mechanism can also be deduced from the surface current distribution as shown in Figs. 6(e) and 6(f), where the colored arrows represent the magnitude and direction of the current. Figures 6(e) and 6(f) show the distributions of current on the top surface of the dielectric at frequencies 25.65 THz and 16.65 THz, respectively. Figures 6(e) and 6(f) indicate that each resonance absorption originates from not only the dipole resonance with the external electric field but also a coupled-mode pair.[23] There are anti-parallel surface current oscillations in the neighboring components, which results from the interaction between the neighboring metallic sides and depends greatly on the distance between them; the greater the distance, the weaker the coupling.[24]

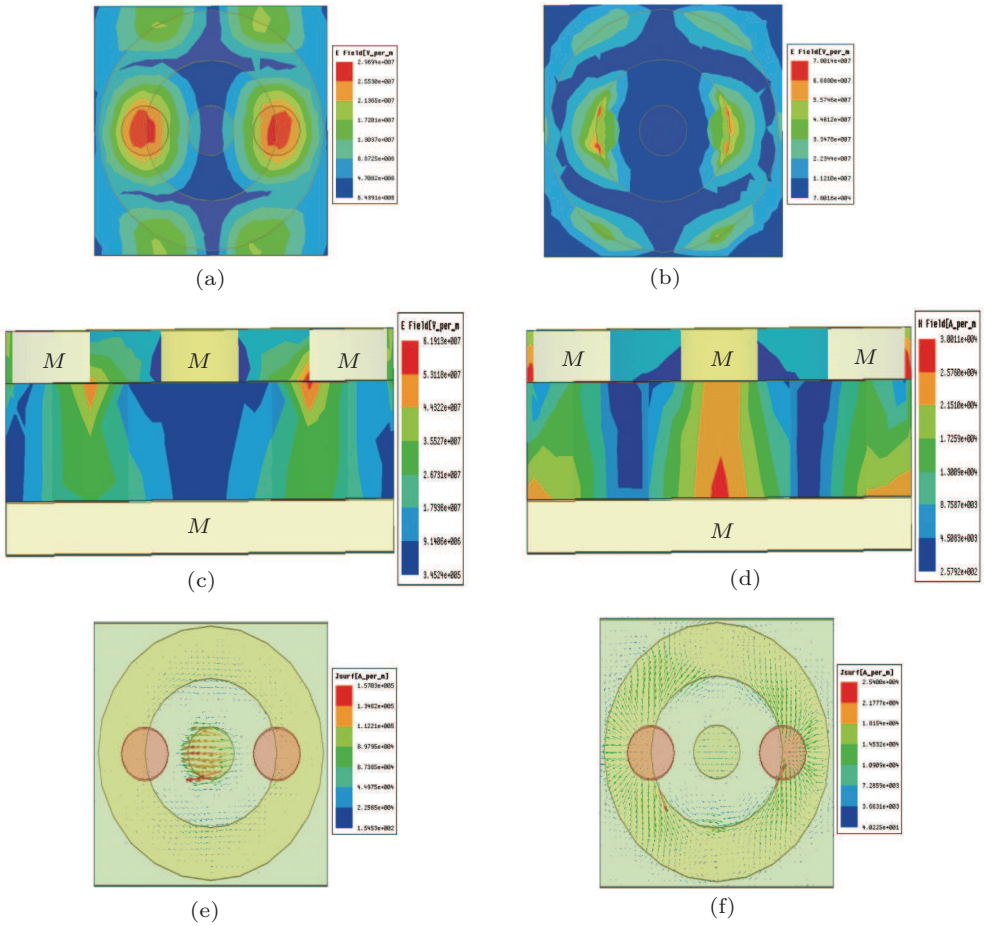


Fig. 6. (color online) Distributions of EM field intensity and current within the double cylindrical cavities at normally incident TM plane wave. (a) Amplitude of electric field in the middle of the dielectric layer in the X–Y plane at $f = 20.65$ THz. (b) Amplitude of electric field on the top of the dielectric layer in the X–Y plane at $f = 20.65$ THz. (c) Amplitude of electric field in the middle of the dielectric layer in the Y–Z plane at $f = 20.65$ THz. (d) Amplitude of magnetic field in the middle of the dielectric layer in the Y–Z plane at $f = 20.65$ THz. (e) and (f) Distributions of current on the top of the dielectric layer in the X–Y plane at $f = 25.65$ THz (e) and $f = 16.65$ THz (f).

3. Conclusions

We numerically studied the near-field enhancement and absorption properties inside the double MDM cylindrical microcavities in the mid-infrared range. For $r_1 = 0.6$ μm, $r_2 = 2.9$ μm, and $r_3 = 1.7$ μm, the values of C are 95%, 97%, and 95% at frequencies 16.65 THz, 20.65 THz, and 25.65 THz, respectively. At $r_4 = 0.01$ μm, Q reaches a maximum ($10^4 \sim 10^5$). We can adjust resonant peaks of interest by changing the structural parameters of the top gold layer. This kind of multi-band absorption, high energy density ratio, flexibility of adjusting resonant peaks, and insensitivity to polarization characteristics make the proposed structures have broad applications in areas such as surface-enhanced spectroscopy, new plasmonic detectors, bio-sensing, solar cells, and so on.

References

[1] Jiang Z H, Yun S, Toor F, Werner D H and Mayer T S 2011 *ACS Nano.* **5** 4641

[2] Shi X Z, Shen C M, Wang D K, Li C, Tian Y, Xu Z C, Wang C M and Gao H J 2011 *Chin. Phys. B* **20** 076103

[3] Du C L, Du C J, You Y M, Zhu Y, Jin S L, He C J and Shi D N 2011 *Appl. Opt.* **50** 4922

[4] Nishijima Y, Nigorinuma H, Rosa L and Juodkazis S 2012 *Opt. Mater. Express* **2** 1367

[5] Schwarz I, Livneh N and Rapaport R 2012 *Opt. Express* **20** 426

[6] He M D, Ma W G and Wang X J 2013 *Chin. Phys. B* **22** 114201

[7] Christensen J, Martin-Moreno L and Garcia-Vidal F J 2010 *Phys. Rev. B* **81** 174104

[8] Lai W C, Chakravarty S, Zou Y and Chen R T 2012 *Opt. Lett.* **37** 1208

[9] Peng P, Huang H, Hu A, Gerlich A P and Zhou Y N 2012 *J. Mater. Chem.* **22** 12997

[10] He X J, Wang Y, Mei J S, Gui T L and Yin J H 2012 *Chin. Phys. B* **21** 044101

[11] Rakhmanov A L, Yampol'skii V A, Fan J A, Capasso F and Nori F 2010 *Phys. Rev. B* **81** 07501

[12] Kocaman S, Aras M S, Hsieh P, McMillan J F, Biris C G, Panoiu N C, Yu M B, Kwong D L, Stein A and Wong C W 2011 *Nat. Photon.* **5** 499

[13] Zimmermann B, Muller T, Meineke J, Esslinger T and Moritz H 2011 *New J. Phys.* **13** 043007

[14] Yuk J M, Park J and Ercius P 2012 *Science* **336** 61

[15] Barnes W L, Dereux A and Ebbesen T W 2003 *Nature* **424** 824

[16] Liu H and Lalanne P 2008 *Nature* **452** 728

[17] Hibbins A P and Sambles J R 2004 *Phys. Rev. Lett.* **92** 147401

[18] Farahani J N, Eisler H J, WPohl D, Pavius M, Fluckiger P, Gasser P and Hecht B 2007 *Nanotechnology* **18** 125506

[19] Curto A G, Volpe G, Taminiau T H, Kreuzer M P, Quidant R and Van-Hulst N F 2010 *Science* **329** 930

[20] Fevillet-Palma C, Todorow Y, Vasanelli A and Sirtori C 2013 *Sci. Rep.* **3** 1361

[21] Fevillet-Palma C, Todorov Y, Steed R, Vasanelli A, Biasiol G, Sorba L and Sirtori C 2012 *Opt. Express* **20** 29121

[22] Liao P F and Wokaun A 1982 *J. Chem. Phys.* **76** 751

[23] Shen X P, Cui T J, Zhao J, Ma H F, Jiang W X and Li H 2011 *Opt. Express.* **19** 9401

[24] Ding P, Liang E J, Zhang L, Zhou Q and Yuan Y X 2009 *Phys. Rev. E* **79** 016604